On Local Singularities in Ideal Potential Flows with Free Surface*

Jian-Guo LIU[1]   Robert L. PEGO[2]

(*Dedicated to Andrew J. Majda on the occasion of his* 70*th birthday*)

Abstract Despite important advances in the mathematical analysis of the Euler equations for water waves, especially over the last two decades, it is not yet known whether local singularities can develop from smooth data in well-posed initial value problems. For ideal free-surface flow with zero surface tension and gravity, the authors review existing works that describe "splash singularities", singular hyperbolic solutions related to jet formation and "flip-through", and a recent construction of a singular free surface by Zubarev and Karabut that however involves unbounded negative pressure. The authors illustrate some of these phenomena with numerical computations of 2D flow based upon a conformal mapping formulation. Numerical tests with a different kind of initial data suggest the possibility that corner singularities may form in an unstable way from specially prepared initial data.

Keywords Incompressible flow, Water wave equations, Splash singularity, Flip-through, Dirichlet hyperbolas, Conformal mapping
2000 MR Subject Classification 76B07, 76B10, 35L67, 30C30

1 Introduction and Background

We consider equations for potential flow of an ideal fluid occupying a region $\Omega_t \subset \mathbb{R}^d$ with smooth boundary at time t, having velocity field $v = \nabla\phi$, pressure p, and constant density $\rho = 1$, that take the following form: For each time t,

$$\Delta\phi = 0 \qquad \text{in } \Omega_t, \tag{1.1}$$

$$\phi_t + \frac{1}{2}|\nabla\phi|^2 + p = 0 \quad \text{in } \Omega_t, \tag{1.2}$$

$$p = 0 \qquad \text{on } \partial\Omega_t. \tag{1.3}$$

These equations are supplemented by the kinematic condition that the fluid domain Ω_t is transported by the velocity. We shall neglect the effects of gravity and surface tension.

It is natural to wonder whether singularities can form in initially smooth solutions of such "zero-gravity water wave" equations. It is well appreciated that the effect of gravity ought to

be negligible at the small scales involved in singularity formation. Physically, surface tension is important on such scales, but we focus here on the mathematical issues that arise in its absence. It is our purpose in this note to review existing work relevant to these issues, and offer numerical evidence that suggests a new scenario for formation of a local singularity.

The initial-value problem for these equations is a difficult fluid free boundary problem, but one that may be treated by the methods developed in the 1990s by Wu [39–40]. For zero-gravity flows with vorticity in smooth bounded domains and smooth enough intial data, smooth solutions for short time have been shown to exist in [10–11, 25].

A few years ago, it was proved by Castro et al. [4–5] that splash singularities can occur, in which, loosely speaking, different parts of a connected body of fluid collide, in a manner similar to how distinct droplets of fluid can collide. It does not seem to be known, however, whether free-surface singularities can form locally without self-intersection in a well-posed initial-value problem for the water wave equations (despite very recent and interesting examples of Zubarev and Karabut [43], discussed below). Recent work of Kinsey and Wu [21] and Wu [41] has provided bounds that constrain singularity formation, and has shown that certain types of free-surface corners present in the initial data persist for short time.

Numerical and experimental evidence and experience suggest a few interesting scenarios that may be associated with local singularities.

Blob splitting For example, can a smoothly evolving single blob of fluid separate in two? One conceivable approach to this problem might involve finding a "least-action" path of incompressible deformations that takes one blob to two. This relates to Arnold's characterization of incompressible Euler flows in fixed domains in terms of least-action paths of volume-preserving diffeomorphisms. Brenier proved in [3, Theorem 2.4], in fact, that smooth Euler flows in a fixed domain satisfy a well-posed relaxed version of Arnold's least-action principle for short time. Zero-gravity free-boundary flows that satisfy (1.1)–(1.3) were formally shown in [26] to be critical paths of action. However, such flows were proved to never be minimizers of the least-action principle, unless they consist of piecewise rigid motions (see[26, Corollary 5.6]).

Flip-through A second scenario, of great physical interest, relates to 2D gravity water waves that break against a vertical wall. This can correspond to a symmetric splash singularity by reflection, with a bubble of 'air' becoming trapped by the free-surface collision. Numerical computations of Cooker and Peregrine [8–9] showed that very high accelerations and strong forces can be produced if the wave is close to breaking but does not break. Instead a sheet or vertical jet of water "flips" up through the trough in front of the steep advancing wave front. See [2, 36, 38] for subsequent discussion and related experiments.

The "flip-through" phenomenon appears to be related to a jet formation phenomenon described by Longuet-Higgins in a series of papers including [27–30]. Analogous to flows with elliptical free boundary that were known to Dirichlet [12], Longuet-Higgins found exact solutions with hyperbolic free boundary, which we will describe in more detail in Section 2. These flows can become singular in finite time, but the way this happens is that the velocity and pre-ssure blow up everywhere in an unbounded domain, while the interface itself remains smooth right up to the limit. Longuet-Higgins pointed out that related solutions with parabolic free boundary were also found by Fritz John [19]. In [30], Longuet-Higgins compared 3D hyperboloidal solutions with experiments on bubbles and breaking waves, and suggested that hyperbolic jets may occur commonly in free-surface flows. (This is consistent with our numerical experiments reported below.) By "zooming out", Longuet-Higgins also described time-varying solutions that contain corners at all times (see [29]).

Self-similar approach to cones or corners It appears that none of the jet-like or flip-through solutions found to date promise to form a true local free-surface singularity. But topological considerations suggest that between the neighboring regimes of bubble-trapping and flip-through, there could be a different, singular behavior. For 3D viscous flows with surface tension, work of D. Lathrop's group in the late 1990s (see [16, 42]) provided numerical and experimental evidence of a self-similar collapse to a free surface with a conical singularity, followed by the self-similar emergence of a thin, high jet of fluid. To our knowledge, no rigorous mathematical analysis of this problem exists, nor has a study of the corresponding inviscid problem without surface tension been carried out.

Acceleration-free interfaces Very recently, Zubarev and Karabut [43] have found analytically a special class of free-boundary solutions of (1.1)–(1.3) which develop a striking variety of local surface singularities. The flows occur in the unbounded 2D domain below a free surface on which fluid particles move ballistically (i.e., with zero acceleration) and purely horizontally. As described in Section 3 below, they are constructed out of the complex Hopf equation (invisicid Burgers equation), with a particular choice of pressure.

Whether these solutions can be considered relevant approximations for singularity development in physical fluids is not clear, however. An issue of concern is that the pressure below the free surface is negative and unbounded below. Thus it may not be possible to approximate these solutions by solutions in bounded domains that satisfy the Taylor sign condition for linear well posedness (see [37]). As invoked in [1], this condition states that the component of the Lagrangian acceleration, in the direction of the outward unit normal n to the fluid domain, strictly exceeds the corresponding component of gravitational acceleration. According to Euler's equations, this means that the pressure satisfies

$$\frac{\partial p}{\partial n} < 0 \quad \text{on } \partial \Omega_t. \tag{1.4}$$

Since the pressure is superharmonic, it must be positive everywhere inside the fluid domain. (This observation was key to Wu's well-posedness theory (see [39–40]).)

The remainder of this paper is organized as follows. In Section 2 we describe in further detail the known exact solutions with hyperbolic free surface in 2D. We describe and discuss the exact solutions of Zubarev and Karabut in Section 3. Then in Section 4 we present a series numerical experiments and illustrations based upon a filtered pseudospectral approximation to a conformal mapping formulation of the system (1.1)–(1.3), as developed and analyzed in work under preparation [24].

Our numerical computations suggest that 2D flows in the borderline regime between bubble trapping and flip-through are highly unstable to the formation of tiny jets (sheets), that likely develop hyperbolic tips consistent with Longuet-Higgins' remarks. We propose, however, that some flows that focus to develop a corner singularity may be stably approximated by time-reversal from flows with near-singular final data. Numerically, by using this strategy we produce a sequence of flows whose interfaces are chosen to approach a corner at the final time, that appear to converge to smooth interfaces at earlier times. By its nature, the numerical evidence is limited, so it remains a challenge for analysis to determine whether such corner singularities can indeed form, or whether some other small-scale instabilities must occur that are not being detected.

2 Dirichlet Ellipsoids and Hyperbolas

In this section we review properties of a family of simple exact solutions to the zero-gravity water wave equations, for use when examining potentially singular features of such flows. We pay particular attention to possible singularities and strong fluid jets (sheets) in 2D flows, but we also note a geodesic interpretation useful in our study of least action principles in [26].

The solutions that we discuss arise from simple straining flows with free surfaces in the form of conic sections. Hyperboloids were previously found by Longuet-Higgins [27] who pointed out that the ellipsoids of Dirichlet [12] are treated in Lamb's treatise (see [22, §382]), where the effects of self-gravitation and rotation are also considered. Other relevant works include [32, 34] (in Russian), which describe ellipsoidal fluid bodies with linear velocity fields (also see [23]). There is a large literature on rotating ellipsoidal fluid bodies with self-gravitation that is not relevant to our purposes here.

2.1 Geodesic curves of conics

Let us proceed to describe some conic free surface potential flows in any dimension $d \geq 2$. To conveniently discuss kinematic relations, we introduce the Lagrangian flow map associated to the velocity field $v = \nabla \phi$, satisfying

$$\dot{X}(z,t) = \nabla\phi(X(z,t),t), \quad X(z,0) = z \tag{2.1}$$

for all $z \in \Omega_0 \subset \mathbb{R}^d$ and all t. In this section all our flows will be incompressible straining flows, corresponding to quadratic potentials of the form

$$\phi(x,t) = \frac{1}{2}\sum_{j=1}^{d} \alpha_j(t)x_j^2 - \beta(t) \quad \text{with} \quad \Delta\phi = \sum_{j=1}^{d} \alpha_j(t) = 0, \tag{2.2}$$

so that the components of the Lagragian map satisfy

$$\dot{X}_j = \alpha_j(t)X_j, \quad j = 1, \cdots, d, \tag{2.3}$$

and the flow is purely dilational along each axis.

Fix a choice of sign $\sigma_j = \pm 1$ for each $j = 1, \cdots, d$, and define, for each $a = (a_1, \cdots, a_d) \in \mathbb{R}_+^d$,

$$S(x,a) = \sum_{j=1}^{d} \sigma_j \frac{x_j^2}{a_j^2}. \tag{2.4}$$

For $\sigma_0 \in \mathbb{R}$, the fluid will be taken to occupy a domain of the form

$$\Omega_t = \{x : S(x,a(t)) < \sigma_0\}. \tag{2.5}$$

The kinematic condition that the boundary flows with the fluid requires

$$0 = \frac{1}{2}\frac{\mathrm{d}}{\mathrm{d}t}S(X,a) = \sum_{j=1}^{d} \sigma_j \frac{X_j^2}{a_j^2}\left(\alpha_j - \frac{\dot{a}_j}{a_j}\right). $$

Leaving degenerate cases aside, it suffices to suppose that

$$\dot{a}_j = \alpha_j a_j, \quad j = 1, \cdots, d. \tag{2.6}$$

Due to the incompressibility constraint in (2.2) it follows that the product

$$a_1 \cdots a_d = r^d \tag{2.7}$$

remains constant in time.

Our main result in this section is the following.

Proposition 2.1 *Given a constant $r > 0$, let $a(t) = (a_1(t), \cdots, a_d(t))$ be any constant-speed geodesic on the surface determined by the relation (2.7) in the space $\mathbb{R}_+^d$ with (possibly indefinite) metric of signature $(\sigma_1, \cdots, \sigma_d)$. Then this determines an ideal potential flow with Ω_t as in (2.5), pressure given by*

$$p(x, t) = \frac{\lambda(t)}{2}(\sigma_0 - S(x, a)), \quad \lambda(t) = \frac{\sum_j \frac{\dot{a}_j^2}{a_j^2}}{\sum_j \frac{\sigma_j}{a_j^2}}, \tag{2.8}$$

and potential ϕ given by (2.2) with $\alpha_j = \frac{\dot{a}_j}{a_j}$ and $\dot{\beta} = \frac{1}{2}\lambda\sigma_0$.

Proof The path $t \mapsto a(t)$ in the indicated surface is a geodesic with constant squared speed $\sum_j \sigma_j \dot{a}_j^2$ if and only if the acceleration $\ddot{a}$ is parallel to the surface normal, meaning here that for some scalar $\lambda = \lambda(t)$,

$$\ddot{a}_j = \frac{\lambda \sigma_j}{a_j}, \quad j = 1, \cdots, d. \tag{2.9}$$

The reason for this is that such a geodesic is a critical path for the augmented action

$$\widetilde{\mathcal{A}} = \int_0^T \sum_j \left(\frac{1}{2}\sigma_j \dot{a}_j^2 + \lambda(t) \log \frac{a_j}{r}\right) \mathrm{d}t.$$

The value of $\lambda(t)$ must be that given in (2.8) due to the requirement that

$$0 = \frac{\mathrm{d}^2}{\mathrm{d}t^2} \sum_j \log a_j = \sum_j \frac{a_j \ddot{a}_j - \dot{a}_j^2}{a_j^2}.$$

Define the potential ϕ by (2.2) using $\alpha_j = \frac{\dot{a}_j}{a_j}$ and $\dot{\beta} = \frac{1}{2}\lambda\sigma_0$ as stated. Then because $\dot{\alpha}_j + \alpha_j^2 = \frac{\ddot{a}_j}{a_j} = \frac{\lambda\sigma_j}{a_j^2}$, the pressure needs to be given by (1.2) as

$$p = -\phi_t - \frac{1}{2}|\nabla\phi|^2 = \dot{\beta} - \frac{1}{2}\sum_j(\dot{\alpha}_j + \alpha_j^2)x_j^2 = \frac{\lambda}{2}(\sigma_0 - S(x, a)).$$

Thus $p = 0$ on $\partial\Omega_t$, and (1.1)–(1.3) all hold, along with the kinematic condition.

We remark that with the present conventions, the Taylor sign condition (1.4) holds exactly when $p > 0$ in Ω_t, and this occurs exactly when $\lambda > 0$ in (2.8).

2.2 Ellipsoidal droplets

In case $\sigma_j = 1$ for all $j = 0, 1, \cdots$, the fluid domains Ω_t always remain bounded and ellipsoidal. These Dirichlet ellipsoids, particularly those corresponding to length-minimizing geodesic paths, played an important role in the study of least action principles for free boundary

flows carried out in [26]. The vector $a(t)$ of semi-major axis lengths moves at a constant (Euclidean) speed and cannot reach any singular point in finite time, so the solution remains smooth globally for $t \in \mathbb{R}$. The pressure $p > 0$ in Ω_t because $\lambda > 0$ in (2.8), so the Taylor sign condition holds, consistent with well-known results on well-posedness for water wave dynamics (see [10, 25, 39–40]). Because $\ddot{a}_j > 0$ for all j, each velocity component $\dot{a}_j$ is increasing, and remains bounded by the speed. Since $\sum \frac{\dot{a}_j}{a_j} = 0$, some component $a_j \to \infty$ as $t \to +\infty$, and some component $a_k \to \infty$ as $t \to -\infty$.

2.3 Ellipsoidal voids

We can consider the fluid to occupy the domain exterior to the ellipsoids above by taking $\sigma_j = -1$ for all j. The pressure $p < 0$ in Ω_t in this case because $\lambda < 0$ in (2.8). By consequence the Taylor sign condition fails and we can expect this 'bubble' flow to be highly unstable.

2.4 Hyperbolas in 2D

In case the σ_j have different signs, the case of two dimensions admits the most simple and complete description. We take $\sigma_0 = \sigma_1 = -1 = -\sigma_2$, so that the domain Ω_t corresponds to

$$\frac{x_1^2}{a_1^2} > 1 + \frac{x_2^2}{a_2^2}. \tag{2.10}$$

The equations of motion derive solely from incompressibility and geodesic speed constraints:

$$a_1 a_2 = r^2, \quad -\dot{a}_1^2 + \dot{a}_2^2 = \widehat{s} \in \mathbb{R}. \tag{2.11}$$

Eliminating $\dot{a}_2$ we find $\dot{a}_1^2(a_2^2 - a_1^2) = \widehat{s}a_1^2$, whence with $\tau = \pm\sqrt{|\widehat{s}|}$ we have

$$\dot{a}_1 = \frac{\tau}{|\tan^2\theta - 1|^{\frac{1}{2}}}, \quad \tan\theta = \frac{a_2}{a_1} = \frac{r^2}{a_1^2}. \tag{2.12}$$

Here $\theta = \theta(t)$ is the angle that the hyperbola's asymptote makes with the x_1 axis.

The pressure from (2.8) has the same sign as λ, which is given here by

$$\lambda = \frac{a_2^2\dot{a}_1^2 + a_1^2\dot{a}_2^2}{a_1^2 - a_2^2} = \frac{2\dot{a}_2^2}{1 - \tan^2\theta}.$$

The pressure is positive and the Taylor sign condition (1.4) holds when $0 < \theta < \frac{\pi}{4}$ ($a_1 > a_2$), and pressure is negative and the Taylor sign condition violated when $\frac{\pi}{4} < \theta < \frac{\pi}{2}$ ($a_1 < a_2$).

Singularities No solution exists globally for $t \in \mathbb{R}$. The solution becomes singular in finite time when $a_1 - a_2$ reaches zero, which means that the asymptotic angle θ reaches $\frac{\pi}{4}$. If initially $\theta < \frac{\pi}{4}$ and $\dot{a}_1 < 0$ the solution becomes singular as t increases, but exists globally for $t < 0$ with $a_1 \to \infty$ as $t \to -\infty$. The same happens if $\theta > \frac{\pi}{4}$ and $\dot{a}_1 > 0$. The reverse happens if $\theta < \frac{\pi}{4}$ and $\dot{a}_1 > 0$, or if $\theta > \frac{\pi}{4}$ and $\dot{a}_1 < 0$—the solution exists globally for $t > 0$ with $a_1 \to \infty$ as $t \to +\infty$.

Approaching a singular time, the free surface shape remains smooth. In case the Taylor sign condition holds and t increases approaching singularity, the angle between the asymptotes widens and approaches $90°$. The pressure and fluid velocity blow up everywhere, since $\alpha_1 = \frac{\dot{a}_1}{a_1}$ blows up. Of course, the domain is unbounded and the energy is infinite, so it is unclear whether this is relevant for any finite energy flow.

Corners No solution we have discussed so far has or develops a free-surface singularity. However, like Longuet-Higgins [29] we obtain a simple flow with a corner by taking $\sigma_0 = 0$, so that for example Ω_t corresponds to the sector of the plane where

$$\frac{x_1}{a_1(t)} > \frac{|x_2|}{a_2(t)}.$$

The same equations (2.11) and (2.12) govern the evolution of the sector opening angle. As above, the Taylor sign condition holds if the corner angle 2θ is less than $90°$ and is violated if it is greater than $90°$. Blowup occurs in the same ways as before. These solutions with corners arise as limits of smooth solutions obtained in the limit $\sigma_0 \uparrow 0$.

We remark that the condition $2\theta < 90°$ is consistent with the theory for water waves with persistent corners developed by Kinsey and Wu [21] and Wu [41], as corners with angles less than $90°$ have the finite "energy" defined in [21] necessary to apply their theory.

3 The Locally Singular Interfaces of Zubarev and Karabut

Very recently, Zubarev and Karabut [43] identified a family of rather explicit ideal fluid flows that provide solutions of the zero-gravity water wave system (1.1)–(1.3) that develop local singularities on the free surface of an unbounded fluid domain. Their study shows that one can construct such solutions out of certain analytic solutions of the complex Hopf equation (inviscid Burgers equation)

$$U_t + UU_z = 0 \quad \text{for } z \in \Omega_t. \tag{3.1}$$

Here we identify $\mathbb{R}^2$ with $\mathbb{C}$ and take $z = x + \mathrm{i}y \in \Omega_t$ to correspond to Eulerian variables in the fluid domain. On the boundary $\partial\Omega_t$ one requires U is real, i.e.,

$$\operatorname{Im} U = 0 \quad \text{on } \partial\Omega_t. \tag{3.2}$$

A solution of (3.1) that is holomorphic in z then corresponds to the holomorphic fluid velocity $U = u - \mathrm{i}v = \phi_x - \mathrm{i}\phi_y$ for a solution of (1.1)–(1.3), provided the pressure satisfies

$$p = -v^2 \quad \text{in } \Omega_t. \tag{3.3}$$

Indeed, one checks directly that the real and imaginary parts of (3.1) yield Euler's equations. We have $u_x + v_y = 0$, $u_y - v_x = 0$, so (3.3) implies $p_x = -2vu_y$, $p_y = -2vv_y$, hence

$$
\begin{aligned}
0 &= (u - \mathrm{i}v)_t + (u - \mathrm{i}v)(u - \mathrm{i}v)_z \\
&= (u_t + uu_x - vv_x) - \mathrm{i}(v_t + uv_x + vu_x) \\
&= (u_t + uu_x - vu_y) - \mathrm{i}(v_t + uv_x - vv_y) \\
&= (u_t + uu_x + vu_y + p_x) - \mathrm{i}(v_t + uv_x + vv_y + p_y).
\end{aligned}
$$

Upon integrating $\phi_x = \operatorname{Re} U$ we obtain ϕ satisfying (1.1)–(1.3).

Along the characteristics $Z(t)$ for (3.1) of course we have

$$\frac{\mathrm{d}Z}{\mathrm{d}t} = U(Z(t), t), \quad \frac{\mathrm{d}}{\mathrm{d}t}U(Z(t), t) = 0.$$

The characteristics are straight lines that do not correspond to fluid particle paths when $v \neq 0$. But on the free surface they do correspond, due to the condition (3.2). Thus fluid particles on

the free surface evolve purely horizontally due to the kinematic condition that the interface is transported by the flow, and ballistically with constant velocity.

Zubarev and Karabut provide several examples of solutions of (3.1) that yield free surfaces that develop local singularities, which arise as local perturbations of the basic solution

$$U = \frac{z}{t} \quad \text{in } \Omega_t = \{x + iy \in \mathbb{C} \mid y < 0\} \text{ with } t < 0. \tag{3.4}$$

This solution describes a simple straining flow with velocity field $(u, v) = \left(\frac{x}{t}, -\frac{y}{t}\right)$, incoming along the x-axis and outgoing along the y-axis for $t < 0$, that blows up everywhere at $t = 0$. Along every characteristic, $Z(t) = Ut \to 0$ as $t \to 0^-$, while every particle path not on the free surface blows up to infinity along the negative y axis.

Perturbations of this solution are found in [43] through implicit solution of characteristic equations expressed in the form

$$z = Ut + F(U), \tag{3.5}$$

where $F(U) \to 0$ as $U \to \infty$ for relevant values of U and one must avoid encountering singularities of F for z in the fluid domain. In the simplest example, $F(U) = \frac{1}{U+i}$ and the free surface is parametrized by the horizontal velocity u via

$$z = tu + \frac{1}{u+i} = tu + \frac{u}{u^2+1} - \frac{i}{u^2+1}, \quad u \in \mathbb{R}. \tag{3.6}$$

In Figure 1 we plot this surface for $t = -4, -3, -2, -1$. For $t < -1$, this surface is a smooth graph $y = \gamma(x, t)$, since $\frac{dx}{du} < 0$ for all u. At $t = -1$, a cusp develops with $y \sim -1 + |x|^{\frac{2}{3}}$. For $t < -1$, the solution $U(z, t)$ maps the domain $y < \gamma(x, t)$ conformally onto the upper half plane $\text{Im } U > 0$. (The vertical velocity $v < 0$ in all of Ω_t, as it is harmonic, negative at ∞, and zero on $\partial \Omega_t$.)
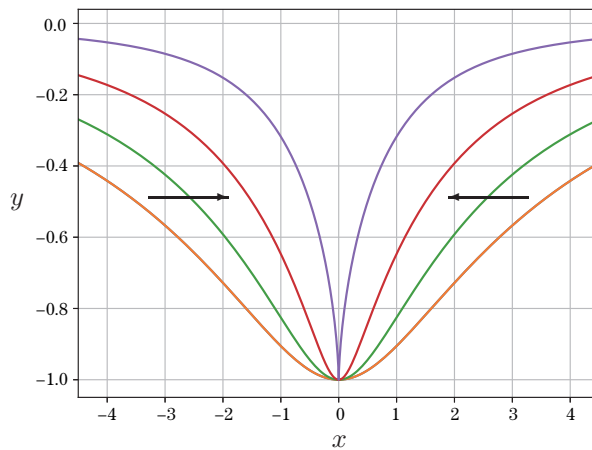

Figure 1 The interface in (3.6) for $t = -4, -3, -2, -1$ (from bottom to top).

While indeed the solutions of [43] satisfy the zero-gravity water wave equations (1.1)–(1.3), it is also true that the free surface experiences zero normal acceleration, with vanishing pressure

gradient:

$$\frac{\partial p}{\partial n} = 0 \quad \text{on } \partial\Omega_t. \tag{3.7}$$

The Taylor sign condition (1.4) does not hold. Moreover, the solutions produced in this way necessarily have $p = -v^2 < 0$ inside the fluid domain Ω_t.

Thus we find it is difficult to imagine how these interesting solutions can arise by local approximation from solutions of well-posed initial-value problems on bounded domains, for which, in the absence of other forcing, (1.4) holds and $p > 0$ in Ω_t. Certainly, if Ω_t is a connected bounded domain, then any holomorphic solution U of (3.1) that satisfies (3.2) is globally constant and the flow is trivial.

4 Computations in 2D

In this section we examine several numerical examples of ideal potential flows that develop from smooth 2D simply connected domains. The general goal is to illustrate and examine how free-surface singularities and jets may develop for such flows. In a number of cases, interfaces that naïvely might have a chance to form local singularities show instead a tendency to form smooth hyperbolic jets. In the last subsection below, however, we produce examples that suggest that corner-forming solutions might be stably generated by time reversal from a sequence of final data that approximate a corner.

4.1 Conformal formulation and a pseudospectral scheme

Our computations are performed using a filtered pseudospectral discretization of a conformal mapping formulation of the equations of motion. A well-known advantage of this formulation is that nonlocal terms involving the Dirichlet-to-Neumann map for the fluid domain become easy to compute when pulled back to the reference domain (here the unit disk $\mathbb{D}$ in the complex plane).

For water wave equations with gravity, conformal mapping formulations of time dependent flows were described and employed for purposes of analysis by, for example, Ovsjannikov [35], Kano and Nishida [20], and Wu [39], and recently by Hunter et al.[18]. For purposes of numerics and formal analysis such conformal formulations were described by Dyachenko et al. [13], Chalikov and Sheinin [6], Choi and Camassa [7], and were extensively developed recently in [14–15, 31].

For the zero-gravity case that we study here, the conformal formulation is described in detail in a forthcoming work (see [24]) joint with Lei Li, which contains a proof of stability and convergence for the spatially discrete filtered scheme. A useful difference from the case of water waves with gravity is that we can exploit Möbius automorphisms of the unit disk $\mathbb{D}$ in order to easily concentrate grid points in a (single) region of high curvature. This simple technique is analogous to a periodic half-strip transformation for water waves described in [31]. However, it is limited in its ability to handle fine-scale features that develop rapidly, as compared, say, to boundary-integral formulations with adaptive grid refinement.

To describe the conformal formulation, we let $z = x + \mathrm{i}y$ denote complex Eulerian coordinates in the fluid domain $\Omega_t \subset \mathbb{C}$, which is parametrized by a conformal map $\mathbf{Z}(\cdot, t) : \mathbb{D} \to \Omega_t$. The fluid boundary $\partial\Omega_t$ is parametrized by $\theta \in \mathbb{T} = \frac{\mathbb{R}}{2\pi\mathbb{Z}}$ via

$$z = \mathbf{Z}(\mathrm{e}^{\mathrm{i}\theta}, t) = X(\theta, t) + \mathrm{i}Y(\theta, t), \quad \theta \in \mathbb{T}.$$

Since $X + iY$ provides the boundary values of a holomorphic function in $\mathbb{D}$, the imaginary part is related to the real part by the Hilbert transform. Expanding

$$X = \sum_{k \in \mathbb{Z}} \widehat{X}_k(t) e^{ik\theta}, \quad Y = \sum_{k \in \mathbb{Z}} \widehat{Y}_k(t) e^{ik\theta},$$

and presuming $\widehat{Y}(0, t) = 0$ for convenience, we have

$$Y = HX, \quad \text{meaning} \quad \widehat{Y}_k(t) = (-i \operatorname{sgn} k) \widehat{X}_k(t).$$

Letting $\Phi(w, t) = \phi(\mathbf{Z}(w, t), t)$ denote the velocity potential represented using conformal coordinates $w \in \mathbb{D}$, the equations of motion take the following form:

$$X_t = (\Lambda X)\frac{\Lambda \Phi}{J} + X_\theta\Big(H\Big(\frac{\Lambda \Phi}{J}\Big) + \mu_0(t)\Big), \tag{4.1}$$

$$\Phi_t = \frac{(\Lambda \Phi)^2 - \Phi_\theta^2}{2J} + \Phi_\theta\Big(H\Big(\frac{\Lambda \Phi}{J}\Big) + \mu_0(t)\Big), \tag{4.2}$$

where $\Lambda = H\partial_\theta$ is the Dirichlet-to-Neumann map for $\mathbb{D}$, having Fourier symbol $\widehat{\Lambda}(k) = |k|$, and $J = X_\theta^2 + (\Lambda X)^2$ is the conformal factor for $\mathbf{Z}$. Above, the value of $\mu_0(t)$ is related to a choice for $\mathbf{Z}(\cdot, t)$, which in principle is free up to some automorphism $\mathbb{D} \to \mathbb{D}$ according to the Riemann mapping theorem. Here we will always take

$$\mu_0(t) \equiv 0,$$

which corresponds to fixing $\mathbf{Z}(0, t)$ and $\arg \mathbf{Z}_w(0, t)$ as constant in time.

We discretize the equations in space by a straightforward pseudospectral scheme using grid points $\theta_j = jh$, $j = 1, \cdots, N$, $h = \frac{2\pi}{N}$. We filter all derivatives by replacing the operator ∂_θ with Fourier symbol ik by $\mathcal{D}_\rho$ with Fourier symbol

$$\widehat{\mathcal{D}}_\rho(k) = ik\,\rho(hk), \quad \rho(\xi) = \exp\Big(-10\Big(\frac{\xi}{\pi}\Big)^{15}\Big).$$

This choice of filter function ρ is similar to that used in [17]. For time integration we use a standard ODE solver in the julia OrdinaryDiffEq package, with tolerances typically set to 10^{-9} or smaller.

4.2 Numerical examples

The accuracy of the numerical scheme was checked, as reported in [24], using an ellipsoidal solution from above together with an explicit conformal map from ellipse to disk given from [33, p. 256] as

$$z = x + iy \mapsto w = \mathbf{Z}^{-1}(z) = \sqrt{k(\rho)}\,\operatorname{sn}\Big(\frac{2K}{\pi}\sin^{-1} z; q\Big), \quad q = \Big(\frac{a-b}{a+b}\Big)^2.$$

Here sn is the Jacobi elliptic function with parameter q.

4.2.1 Five-fold symmetric initial velocity

Taking the initial shape as circular with initial parametrization and 5-fold symmetric initial velocity potential given by

$$\mathbf{Z}_0(w) = w, \quad \Phi_0(\theta) = -0.15 \cos 5\theta,$$

the solution was computed with $N = 1024$ grid points and the image $Z = X + iY$ is plotted at time $t = 0.21$ in Figure 2, together with a quiver plot of the velocity at every 2nd grid point. The fluid domain develops protuberances that may be developing into jets or corners. The arrows, which indicate the velocity at alternate grid points, have become fairly widely separated near the tips. Further computation becomes difficult with a uniformly spaced grid, as the conformal grid becomes stretched rapidly as the tips develop.
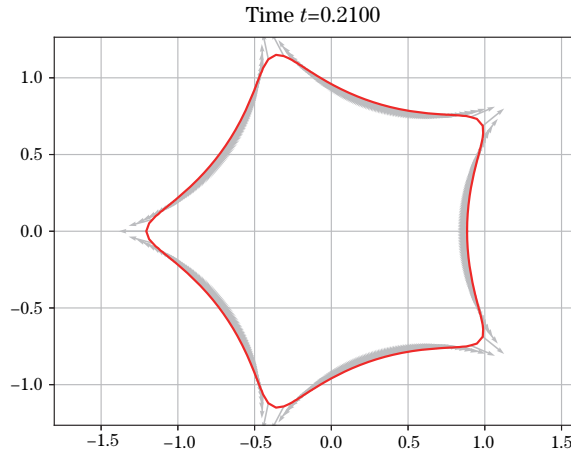
Figure 2 Droplet shape with five-fold symmetric initial velocity.

4.2.2   Unimodal initial velocity

In order to examine more closely whether fluid protuberances may develop corner singularities, we consider a unimodal initial velocity, and take the initial shape as a circle but parametrize it using a Möbius transformation with parameter r:

$$\mathbf{Z}_0(w) = \zeta_r(w) := \frac{w + r}{1 + rw}, \quad \Phi_0(\theta) = \left(\frac{X_0(\theta) + 1}{2}\right)^5.$$ (4.3)

We take $r \approx 0.881$ corresponding to compressing the grid by a factor of

$$c = \left(\frac{1 + r}{1 - r}\right)^2 = 250$$ (4.4)

near $\theta = 0$ relative to that near $\theta = \pi$.

The fluid domain computed at time $t = 0.6$ with $N = 1024$ points is plotted in Figure 3, together with a hyperbola determined by fitting 150 values of Y^2 to a quadratic function of X using the polyfit function in julia. The hyperbola's asymptotes are also plotted. The hyperbola takes the form

$$\frac{(x - x_0)^2}{a^2} + \frac{y^2}{b^2} = 1, \quad a = 0.532, \ b = 0.199, \ x_0 = 2.398.$$ (4.5)

The fit of the hyperbola to the (Pinocchio-like) "nose" growing from this droplet is remarkably good. This suggests that the nose will grow indefinitely with shrinking angle between the
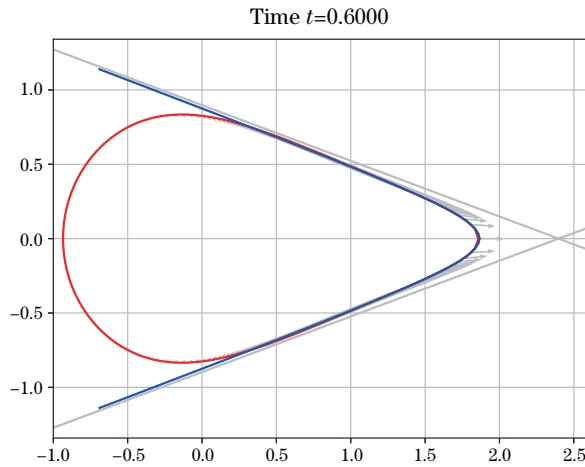
Time t=0.6000

Figure 3 Unimodal initial velocity with tip fit to hyperbola.

asymptotes, like the exact Dirichlet-hyperbola solutions found by Longuet-Higgins that were described in Section 2. Thus we expect the solution to remain smooth for all later time and never form a corner singularity.
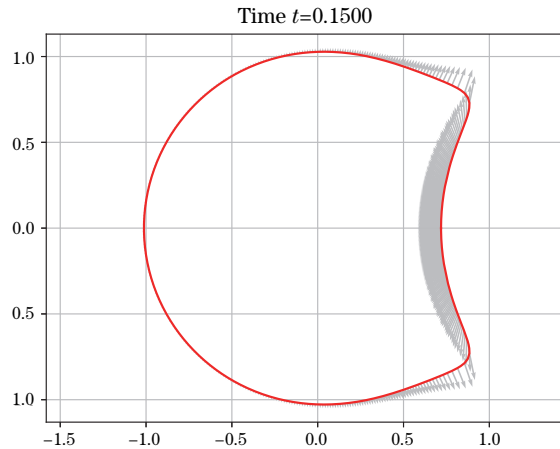
4.2.3 Unimodal compression

Time t=0.1500

Figure 4 Solution with reversed unimodal initial velocity.

In many other cases that we have tried, similar nose-like protuberances emerge that appear likely to develop a hyperbolic shape, consistent with Longuet-Higgins's suggestion (see [30]) that "hyperbolic jets may occur commonly in free surface flows". It is difficult for us to study this phenomenon quantitatively, though, due to rapid stretching of the conformal grid. For example,

in Figure 4 we plot the result of simply reversing the sign of the initial velocity potential in (4.3) and starting with the same circular initial shape but with weaker grid compression ratio $c = 2$. Two proto-jet-like bulges emerge on the sides of the resulting indentation.
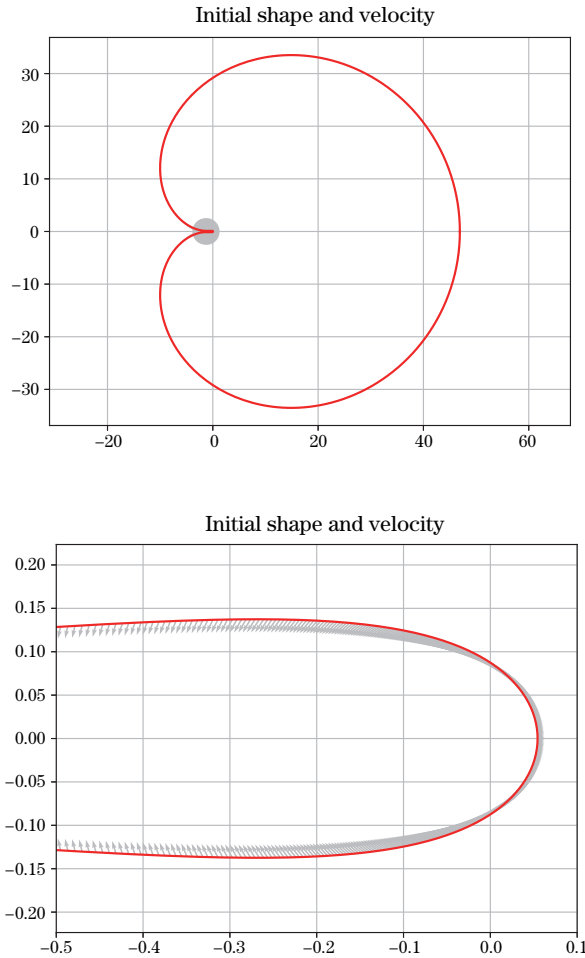
4.2.4 Splash singularity

Figure 5 Initial data for a splash singularity.

We can compute a domain boundary curve that self-intersects in finite time (corresponding to a "splash singularity" (see [4–5]) if we start, not with a circular shape, but with one close to self-intersecting as in Figure 5 (with zoom-in shown as well) and with appropriate initial velocity. In particular, we take initial data given in terms of the circle parametrization $\mathbf{Z}_0$ in (4.3) by

$$X_0(\theta) = \operatorname{Re}(\mathbf{Z}_0(\mathrm{e}^{\mathrm{i}\theta}) + 1.5)^{4.2} \tag{4.6}$$

with $r = -0.4776$, and take the initial conformal potential in the form

$$\Phi_0(\theta) = 0.45\left(\frac{X_0(\theta) - 1.2}{2}\right)^7 - \left(\frac{X_0(\theta) - 1.2}{2}\right)^3. \tag{4.7}$$

The zoomed-in image curves $X + iY$ for the solution at times $t = 0.6$ and 0.64 are shown in Figure 6. The computed solution loses physical meaning after the first time of self-intersection in between, but computationally there appears to be no breakdown of regularity in the solution of the system (4.1)–(4.2) that governs evolution of the interfacial curve. Instead two jet-like bulges appear that are rather similar to those in Figure 4, which plausibly develop into hyperbolic jets that may forever remain smooth.
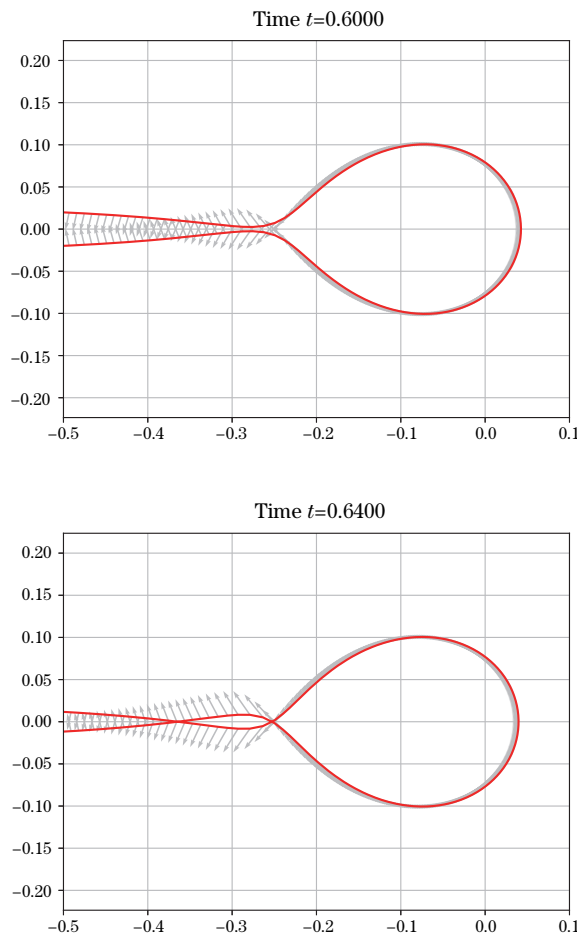
Figure 6   Solution before and after self-intersection.

4.2.5   Emerging jet

Figure 7 is a zoom-in on the computed shape at time $t = 0.19$ using the same initial shape
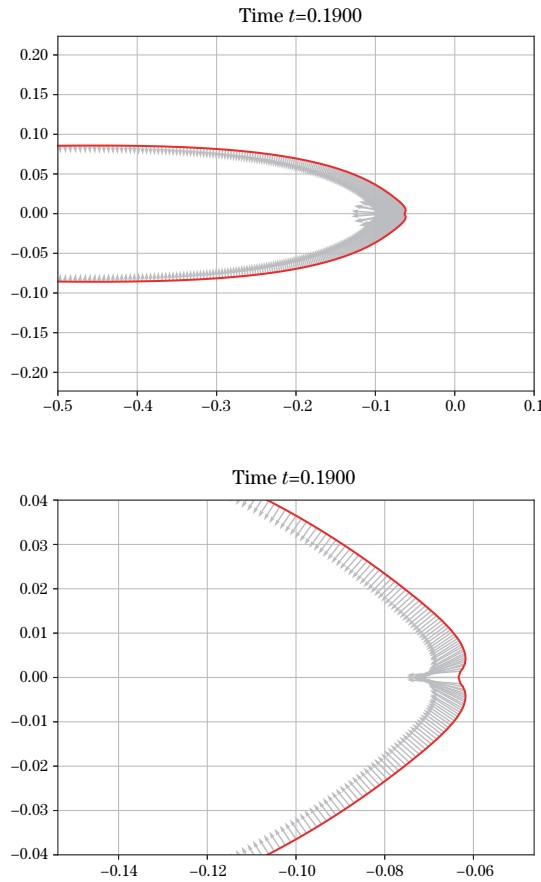
Figure 7 Solution with emerging jet, extra zoom-in on right.

as for the splash above but with the slightly different initial velocity potential

$$\Phi_0(\theta) = 0.45\Big(\frac{X_0(\theta) - 1.2}{2}\Big)^7 - 1.2\Big(\frac{X_0(\theta) - 1.2}{2}\Big)^3. \tag{4.8}$$

On the scales of Figure 5, little difference can be seen at this time. However the zoom-in reveals that a tiny, strong emerging jet is developing here. The computation cannot be continued much beyond this time due to the rapid spreading of the conformal grid.

This jet recalls the "flip-through" behavior found by Cooker and Peregrine [8–9] who used boundary-integral methods to compute free-surface water waves with gravity. Close to a critical case when an overturning wave impacts a vertical wall, these authors found fast-accelerating jets that emerge vertically along the wall.

4.3 Approximating corner formation via time reversal

The foregoing computations demonstrate the difficulties of exploring for local singularity formation by direct integration that interpolates between splash-singularity formation and smooth flip-through. As illustrated in §4.2.5, in a region of convergence flow with high interfacial curva-

ture, the interface appears to develop instability to jet formation leading to flip-through. Thus it seems difficult to identify whether local singularities can form through this direct numerical approach.

In this section we pursue a different approach to investigate local singularity formation as time increases. As the governing equations are time-reversible, we investigate instead whether an initial interface that contains a corner can expand to become smooth for positive time.

To investigate this with a code designed for smooth solutions in a domain parametrized by the unit disk, we take a sequence of smooth initial interfaces that approximate one with a corner, and we study whether the solutions at fixed times $t > 0$ converge. We find that we get good evidence of convergence by taking the initial velocity roughly normal to the interface in the vicinity of the corner.

The initial data for our computations are taken to approximate an initial wedge-shaped domain Ω_Θ with opening angle $\Theta \in (0, \pi)$ (as measured in the 'air'). This wedge is the image of the right half-plane $\operatorname{Re} w > 0$ under the map

$$\zeta_\Theta(w) := w^p, \quad p = 2 - \frac{\Theta}{\pi} \in (1, 2). \tag{4.9}$$

Corresponding to this wedge domain, the power-law complex velocity potential

$$f_\Theta(z) = z^{\frac{1}{p}} \tag{4.10}$$

produces a velocity field (u, v) via $u + iv = \overline{f'_\Theta(z)} = \frac{\overline{z}^{\frac{1-p}{p}}}{p}$ which is normal to the interface $\partial\Omega_\Theta = (i\mathbb{R})^p$, since $\arg z = \frac{\pi}{2} p$ implies $\arg(u + iv) = \frac{\pi}{2}(p - 1) = \arg z - \frac{\pi}{2}$.

We approximate the wedge by parametrizing the initial interface in terms of $w = e^{i\theta}$ via

$$\mathbf{Z}_0(w) = \zeta_\Theta \circ \zeta_a \circ \zeta_b \circ \zeta_r(w). \tag{4.11}$$

Here ζ_r is the Möbius transformation from (4.3) that reparametrizes the unit circle to redistribute points, and the function

$$\zeta_b(w) := -1 + \frac{2(1 + b)}{2 + b(1 - z)} \tag{4.12}$$

conformally maps the unit disk $\mathbb{D}$ to a large disk in the right half plane that intersects the real axis at 0 and $b \gg 1$. Then for small $a > 0$, the map

$$\zeta_a(w) := \frac{1}{2} w + \sqrt{\left(\frac{1}{2} w + a\right)^2 + 3a^2} - a \tag{4.13}$$

conformally takes the right half plane strictly inside itself, with $\operatorname{Re} \zeta_a(w) > 0$ for $\operatorname{Re} w > 0$,

$$\zeta_a(0) = a, \quad \zeta_a(w) = w + o(1) \quad \text{as } |w| \to \infty. \tag{4.14}$$

With this parametrization, the initial interface intersects the real axis at the points

$$x_0 = \mathbf{Z}_0(-1) = a^p, \quad x_1 = \mathbf{Z}_0(1) = \zeta_a(b)^p \approx b^p. \tag{4.15}$$

In our computations, we take the actual initial complex velocity potential to be

$$f_0(z) = f_\Theta(z) - \mu z, \quad \mu = f'_\Theta(x_1),$$

where μ is chosen to make the initial velocity vanish at the x-intercept x_1.

In total, the initial data for the system (4.1)–(4.2) takes the form

$$X_0(\theta) = \operatorname{Re} \mathbf{Z}_0(e^{i\theta}), \quad \Phi_0(\theta) = \operatorname{Re} f_0(\mathbf{Z}_0(e^{i\theta})). \tag{4.16}$$

Parameters For all the computations we report, we discretize $\theta \in [0, 2\pi)$ using $N = 4096$ points. The grid compression ratio $c = 15$ in (4.4) determines $r \approx 0.5895738$, and we always compute b to satisfy $b^p = 1000$ so that $x_1 \approx 1000$. The initial interface and velocity field corresponding to $\Theta = 90^0$, $x_0 = 0.002$ is plotted in Figure 8.
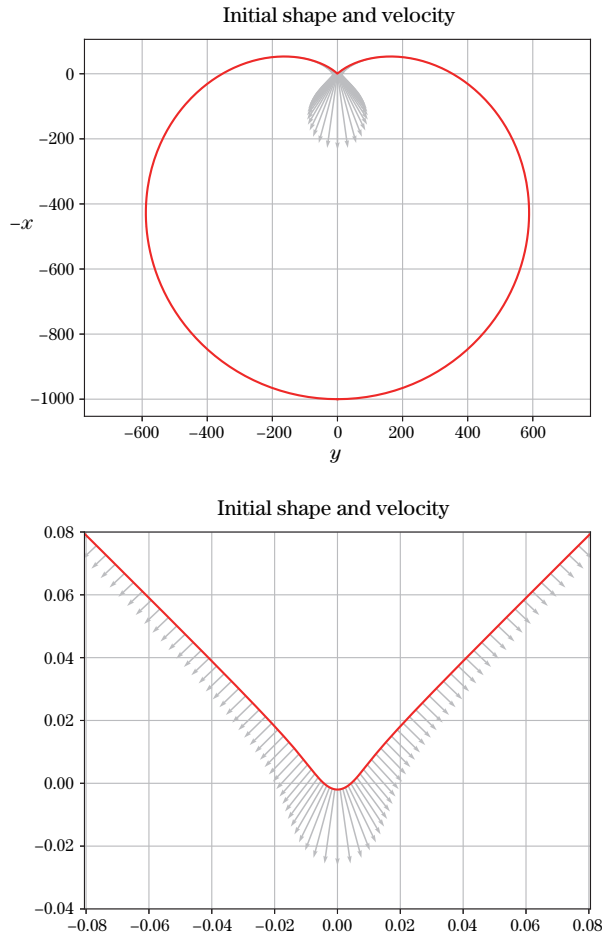

Figure 8 Initial interface and velocity for $\Theta = 90°$, $x_0 = 0.002$.

Results For all of our results in this section, we plot $-X$ vs Y to simulate "fluid underneath air". In Figures 9, 10 and 11 we report results corresponding to $\Theta = 27°$, $90°$ and $153°$

respectively. In each figure, the interface is plotted at 5 equispaced times from 0 to 2, and at each of these times the solutions for $x_0 = 0.002$ (solid), 0.005 (dashed) and 0.01 (dotted) are plotted.
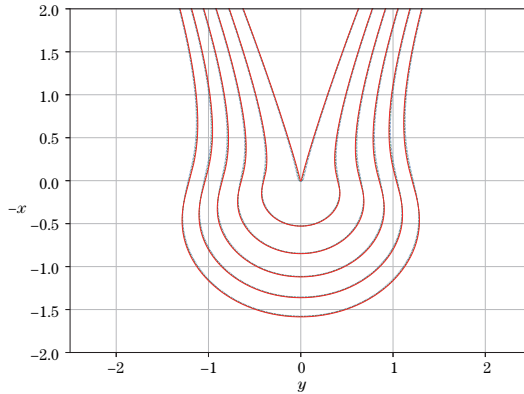

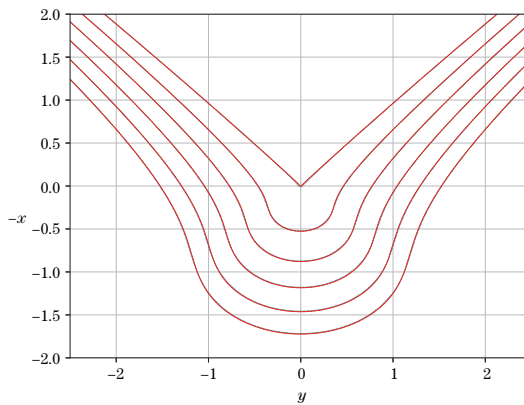Figure 9 Interface for $t = 0.4k$ $(0 \leq k \leq 5)$ with $\Theta = 27°$, $x_0 = 0.002, 0.005, 0.01$.

Figure 10 Interface for $t = 0.4k$ $(0 \leq k \leq 5)$ with $\Theta = 90°$, $x_0 = 0.002, 0.005, 0.01$.

The interfaces for the same times but different values of x_0 are barely distinguishable (though one can zoom in online to see some difference). Thus it appears plausible that in the limit $x_0 \downarrow 0$, the solutions for fixed positive $t > 0$ may converge. If so, then upon time reversal, the final interfaces would converge to one with a corner at $z = 0$. (We remark that in our computations, upon reversing the velocity at $t = 2$ and continuing, we recover the initial data to maximum-norm accuracy of order 10^{-6} in both position and potential in all cases.)

In Figure 12 we study the convergence of the interface position as a function of x_0, for $\Theta = 90°$ at $t = 1$. In the left panel we plot absolute differences in position $Z = X + iY$ for grid points with label $j = 1025$ to 3072. Writing $Z(x_0)$ to indicate the dependence on the initial
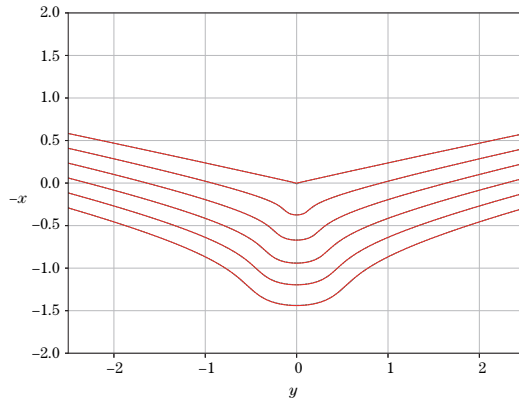
Figure 11 Interface for $t = 0.4k$ $(0 \le k \le 5)$ with $\Theta = 153°$, $x_0 = 0.002, 0.005, 0.01$.
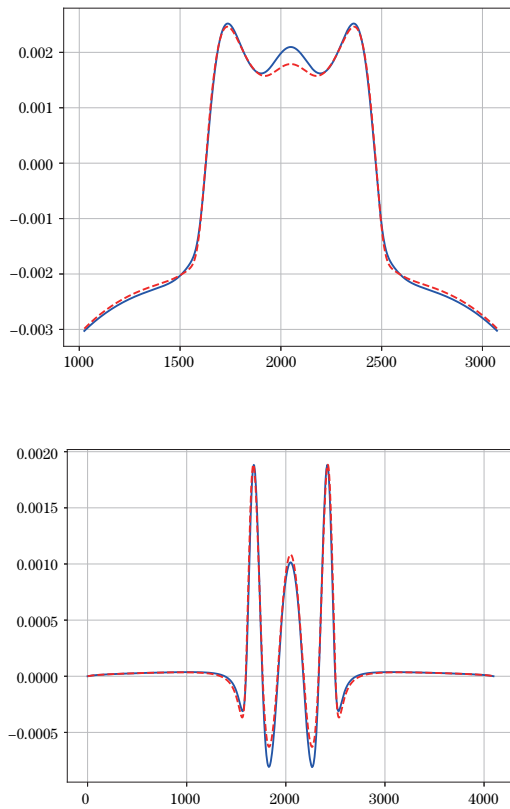

Figure 12 Convergence study for $\Theta = 90°$, $x_0 = 0.002, 0.004, 0.006$. Left: Absolute position errors in $z(x_0)$ at grid points 1025–3072. $|z(.004) - z(.002)|$ (solid), $\frac{1}{2}|z(.006) - z(.002)|$ (dashed). Right: Similar velocity errors, relative to $v_{\max} = 0.782725$.

intercept, we plot $|Z(0.004) - Z(0.002)|$ and $\frac{1}{2}|Z(0.006) - Z(0.002)|$. The rough agreement of these quantities is consistent with linear convergence as $x_0 \downarrow 0$. This can be expected, as the origin of time is not adjusted for different x_0. In the right panel we plot similar errors in complex velocity, relative to the maximum velocity at $t = 1$.
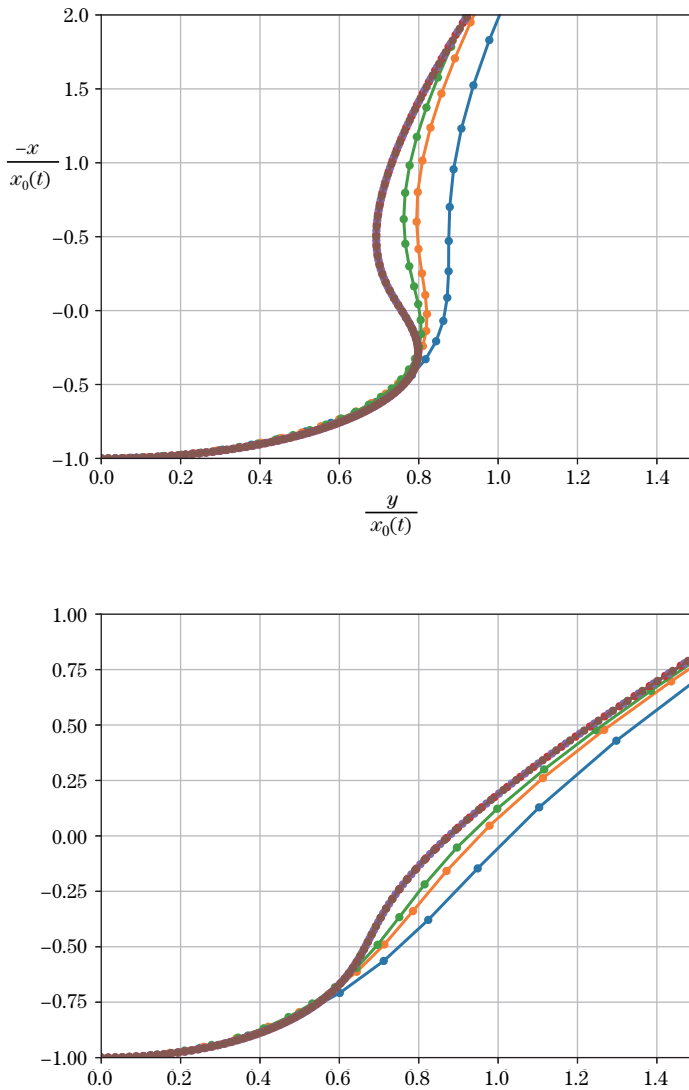

Figure 13 Scaled interfaces for $\Theta = 27°$ (left) and $90°$ (right), plotted for times $t = 0.004k$ and $0.2 - 0.004k$, $k = 1, 2, 3$. Arrows indicate direction of motion in increasing time.

Self-similarity In our computations, the interface appears to expand away from the wedge with roughly a locally self-similar shape. See Figure 13, where for $\Theta = 27°$ and $90°$ we plot the interfaces $X + \mathrm{i}Y = \mathbf{Z}(\mathrm{e}^{\mathrm{i}\theta}, t)$ scaled by the x-intercept $x_0(t) := X(\pi, t) = \mathbf{Z}(-1, t)$ corresponding
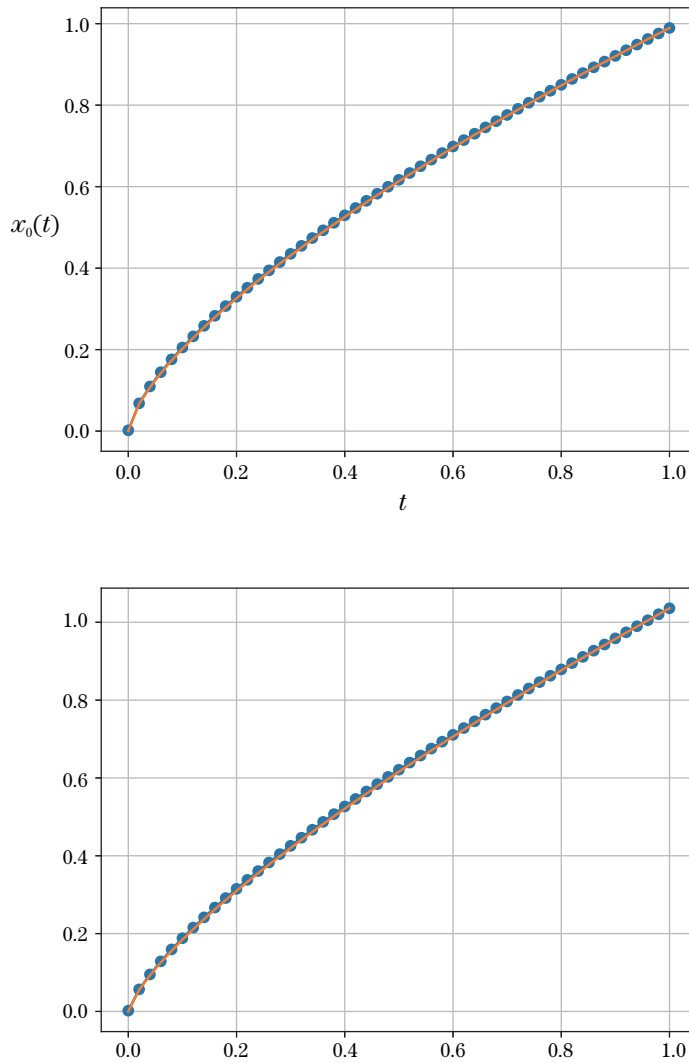
Figure 14 Smallest x-intercept of interface vs. t (dots), compared to a power law ct^α matching at $t = 1$. Left: $\Theta = 27°$, $\alpha = 0.69$. Right: $\Theta = 90°$, $\alpha = 0.75$.

to $X(\pi, 0) = x_0(0) = 0.002$. The interfaces are plotted at 3 equispaced times $t_k = 0.004k$ $(k = 1, 2, 3)$ then again at 3 later equispaced times $0.2 - t_k$. Arrows indicate the direction of interface motion as time increases.

The plots at the later times are hardly distinguishable. This suggests that a locally scale invariant shape develops.

The local scale of the solution also appears to follow a power law growth in time, as suggested by the plots in Figure 14. Here, for $\Theta = 27°$ and $90°$, we plot the smallest x intercept as a

function of t. The markers indicate the numerically computed solution; the solid lines are plots of ct^{α} with c adjusted to match at $t = 1$, the different values $\alpha = 0.69$ (for $\Theta = 27°$) and 0.75 (for $\Theta = 90°$).

Evidently a deeper analysis of the development of a self-similar solution would be desirable. We point out that if indeed a solution exists with x-intercept proportional to t^{α}, then the interfacial acceleration at this point would blow up like $t^{\alpha-2}$.

5 Discussion

For ideal potential flow in 2D, despite the lack of any regularizing effect from surface tension, viscosity or gravity, our numerical experience is that a smooth fluid boundary does not readily form corner singularities when protuberances emerge from the main body of fluid. Instead, consistent with the suggestion of Longuet-Higgins, the shape of such a "nose" was found to approach that of a hyperbola, with asymptotes that narrow with increasing time. Dirichlet hyperbola solutions of this type persist and remain smooth forever.

In §4.3, we identified a possible class of solutions having smooth initial data that approximate a corner, and yield solutions that appear to converge and remain smooth for $t > 0$. The (exterior) angle Θ of the corner appears to make no difference over a wide range in $\left(0, \frac{\pi}{2}\right)$. Further, the initial development of the interface appears to rapidly approach a locally self-similar shape in the vicinity of the corner. Whether such a limiting singular solution or self-similar solution truly exists is an interesting question, but one which remains open for future investigation.

References

[1] Beale, J., Hou, T. and Lowengrub, J., Growth rates for the linearized motion of fluid interfaces away from equilibrium, *Commun. Pur. Appl. Math.*, **46**, 1993, 1269–1301.

[2] Bredmose, H., Hunt-Raby, A., Jayaratne, R. and Bullock, G. N., The ideal flip-through impact: Experimental and numerical investigation, *J. Engrg. Math.*, **67**, 2010, 115–136.

[3] Brenier, Y., Minimal geodesics on groups of volume-preserving maps and generalized solutions of the Euler equations, *Comm. Pure Appl. Math.*, **52**, 1999, 411–452.

[4] Castro, A., Córdoba, D., Fefferman, C. L., et al., Splash singularity for water waves, *Proc. Natl. Acad. Sci. USA*, **109**, 2012, 733–738.

[5] Castro, A., Córdoba, D., Fefferman, C. L., et al., Finite time singularities for the free boundary incompressible Euler equations, *Ann. of Math.* (2), **178**, 2013, 1061–1134.

[6] Chalikov, D. and Sheinin, D., Numerical modeling of surface waves based on principal equations of potential wave dynamics, Technical Note NOAA/NCEP/OMB, 1996, 54 pages.

[7] Choi, W. and Camassa, R., Exact evolution equations for surface waves, *J. Engr. Mech.*, **125**, 1999, 756–760.

[8] Cooker, M. and Peregrine, D., Computations of violent motion due to waves breaking against a wall, *Proc. 22nd Intl. Conf. on Coastal Engineering*, ASCE, 1990, 164–176.

[9] Cooker, M. J. and Peregrine, D. H., Violent Motion as Near Breaking Waves Meet a Vertical Wall, Breaking Waves, Springer-Verlag, Berlin, Heidelberg, 1992, 291–297.

[10] Coutand, D. and Shkoller, S., Well-posedness of the free-surface incompressible Euler equations with or without surface tension, *J. Amer. Math. Soc.*, **20**, 2007, 829–930.

[11] Coutand, D. and Shkoller, S., A simple proof of well-posedness for the free-surface incompressible Euler equations, *Discrete Contin. Dyn. Syst. Ser. S*, **3**, 2010, 429–449.

[12] Dirichlet, G. L., Untersuchungen über ein Problem der Hydrodynamik, *Abh. Kön. Gest. Wiss. Göttingen (Abh. math.)*, **8**, 1860, 3-42.

[13] Dyachenko, A. I., Zakharov, V. E. and Kuznetsov, E. A., Nonlinear dynamics of the free surface of an ideal fluid, *Plasma Phys. Rep.*, **22**, 1996, 829–840.

[14] Dyachenko, S. and Newell, A. C., Whitecapping, *Stud. Appl. Math.*, **137**, 2016, 199–213.

[15] Dyachenko, S. A., Lushnikov, P. M. and Korotkevich, A. O., Branch cuts of Stokes wave on deep water, Part I: Numerical solution and Padé approximation, *Stud. Appl. Math.*, **137**, 2016, 419–472.

[16] Hogrefe, J. E., Peffley, N. L., Goodridge, C. L., et al., Power-law singularities in gravity-capillary waves, *Phys. D.*, **123**, 1998, 183–205.

[17] Hou, T. Y. and Li, R., Computing nearly singular solutions using pseudo-spectral methods, *J. Comput. Phys.*, **226**, 2007, 379–397.

[18] Hunter, J. K., Ifrim, M. and Tataru, D., Two dimensional water waves in holomorphic coordinates, *Comm. Math. Phys.*, **346**, 2016, 483–552.

[19] John, F., Two-dimensional potential flows with a free boundary, *Comm. Pure Appl. Math.*, **6**, 1953, 497–503.

[20] Kano, T. and Nishida, T., Sur les ondes de surface de l'eau avec une justification mathématique des équations des ondes en eau peu profonde, *J. Math. Kyoto Univ.*, **19**, 1979, 335–370.

[21] Kinsey, R. H. and Wu, S., A priori estimates for two-dimensional water waves with angled crests, *Camb. J. Math.*, **6**, 2018, 93–181.

[22] Lamb, H., Hydrodynamics, Cambridge Mathematical Library, Cambridge University Press, Cambridge, 6th ed., with a foreword by R. A. Caflisch (Russel E. Caflisch), 1993.

[23] Lavrenteva, O. M., Motion of a liquid ellipsoid, *Dokl. Akad. Nauk SSSR*, **253**, 1980, 828–831.

[24] Li, L., Liu, J.-G. and Pego, R. L., Numerical analysis of a conformal mapping formulation for incompressible fluid drops, in preparation.

[25] Lindblad, H., Well-posedness for the motion of an incompressible liquid with free surface boundary, *Ann. of Math.* (2), **162**, 2005, 109–194.

[26] Liu, J.-G., Pego, R. L. and Slepčev, D., Least action principles for incompressible flows and optimal transport between shapes, 2016, arXiv:1604.03387.

[27] Longuet-Higgins, M. S., A class of exact, time-dependent, free-surface flows, *J. Fluid Mech.*, **55**, 1972, 529–543.

[28] Longuet-Higgins, M. S., Self-similar, time-dependent flows with a free surface, *J. Fluid Mech.*, **73**, 1976, 603–620.

[29] Longuet-Higgins, M. S., On the forming of sharp corners at a free surface, *Proc. Roy. Soc. London Ser. A*, **371**, 1980, 453–478.

[30] Longuet-Higgins, M. S., Bubbles, breaking waves and hyperbolic jets at a free surface, *J. Fluid Mech.*, **127**, 1983, 103–121.

[31] Lushnikov, P. M., Dyachenko, S. A. and Silantyev, D. A., New conformal mapping for adaptive resolving of the complex singularities of Stokes wave, *Proc. A.*, **473**, 2017, 19 pages.

[32] Nalimov, V. I. and Pukhnachev, V. V., Nonstationary motion of a perfect fluid with a free boundary, Unpublished Lecture Notes, Novosibirsk Gos. Univ., Novosibirsk, 1975 (in Russian).

[33] Nehari, Z., Conformal mapping, Dover Publications, Inc., New York, 1975.

[34] Ovsjannikov, L. V., A class of nonsteady motions of an incompressible fluid, Proceedings of the Fifth Session of the Scientific Council on the Use of Detonation in the National Economy, Ilim, Frunze, 1965, 34–42 (in Russian).

[35] Ovsjannikov, L. V., A plane problem on the unsteady motion of an incompressible fluid with a free boundary, *Dinamika Splošn. Sredy*, 1971, 22–26.

[36] Peregrine, D. H., Water-wave impact on walls, in Annual review of fluid mechanics, *Annu. Rev. Fluid Mech.*, **35**, 2003, 23–43.

[37] Taylor, G., The instability of liquid surfaces when accelerated in a direction perpendicular to their planes, I, *Proc. Roy. Soc. London. Ser. A.*, **201**, 1950, 192–196.

[38] Wang, A., Ikeda-Gilbert, C. M., Duncan, J. H., et al., The impact of a deep-water plunging breaker on a wall with its bottom edge close to the mean water surface, *J. Fluid Mech.*, **843**, 2018, 680–721.

[39] Wu, S., Well-posedness in Sobolev spaces of the full water wave problem in 2-D, *Invent. Math.*, **130**, 1997, 39–72.

[40] Wu, S., Well-posedness in Sobolev spaces of the full water wave problem in 3-D, *J. Amer. Math. Soc.*, **12**, 1999, 445–495.

[41] Wu, S., A blow-up criteria and the existence of 2d gravity water waves with angled crests, 2015, arXiv:1502.05342.

[42] Zeff, B. W., Kleber, B., Fineberg, J. and Lathrop, D. P., Singularity dynamics in curvature collapse and jet eruption on a fluid surface, *Nature*, **403**, 2000, 401.

[43] Zubarev, N. M. and Karabut, E. A., Exact local solutions for the formation of singularities on the free surface of an ideal fluid, *JETP Lett.*, **107**, 2018, 412–417.